HERON

HERON contains contributions based mainly on research work performed in I.B.B.C. and STEVIN and related to strength of materials and structures and materials science.

Volume 17 (1970) no. 3

CONTENTS:

Jointly edited by:

STEVIN - Laboratory of the Department of Civil Engineering of the Technological University, Delft, The Netherlands
and
I.B.B.C. Institute TNO for Building Materials and Building Structures, Rijswijk (ZH), The Netherlands.

S U M M E R Y

In studying the effect of uniaxial tensile stressing on Poissons' ratio of concrete, difficulties arise in measuring the very small lateral strains. To obtain high sensitivity, as required for accurate determinations, an optical measuring device has been conceived and build, which is provided with two plane mirrors enclosing a small angle.

By this means, a number of reflections of about 16 is attainable. In climatized surroundings, reliable registrations of differences in strain as small as 0,025 μstr. are within reach.

Although influenced by fluctuations in the atmosphere, tests have demonstrated that it is possible, without even controlling temperature, to find fairly good results.

The purpose was to show that it is possible to detect a discontinuity point in the development of Poissons' ratio for concrete in tension. The derivative of the volume contraction, with respect to the strain, which is directly related to Poissons' ratio, is the most suitable parameter for this purpose.

To investigate the effect of a lateral compression in a uniform stressfield upon Poissons' ratio in tension, a simple biaxial bending experiment can be performed.

When rhombic plates are supported in opposite corners and loaded in the free corners they will produce an anticlastic homogeneous bending situation. By varying the diagonal length ratio a number of different stressfields will result. Again, Poissons' ratio can be used to formulate a limitstate.

To investigate the handiness of moiré techniques, a (Ligtenberg) reflection method and a shadow moiré method are applied on perspex.

By controlled strain testing of a brittle material (i.e. concrete) very high strains are obtainable resulting in dense but inhomogeneous crackpatterns. Full field methods like moiré techniques give an integral view of the deformations, offering the possibility to relate Poissons' ratio to the disrupture process, f.e. the starting of this process can be associated with the discontinuity point in Poissons' ratio.

Especially the shadow moiré technique offers this possibility with rather simple and cheap apparatus.

S A M E N V A T T I N G

Twee optische methoden die in het Stevin-laboratorium zijn toegepast om de dwarscontractie-coëfficiënt te bepalen van perspex en micro-beton die onderworpen worden aan een éénassige trekspanning en een anticlastische buigspanningstoestand.

Bij het bestuderen van het verloop van de dwarscontractie-coëfficiënt bij een éénassige beproeving op trek doet zich het probleem voor de zeer kleine vervormingen in dwarsrichting te moeten registreren.

Daarom is een optische meetapparatuur ontwikkeld met een grote gevoeligheid. Deze gevoeligheid wordt bereikt door twee spiegels met een geringe openingshoek toe te passen. Binnen dit spiegelsysteem kan een lichtbundel ongeveer 16 maal reflecteren.

Op deze wijze kunnen in een geconditioneerde ruimte waarden voor de rek tot 0,025 µrek vastgesteld worden. Ook in niet-geconditioneerde ruimten zijn redelijk goede beproevingsresultaten bereikt.

De opzet was een discontinuïteit aan te tonen in het verloop van de dwarscontractie-coëfficiënt bij een beproeving op éénassige trek. De meest geschikte parameter daarbij is de afgeleide maar de rek van de volumerek, die op zich rechtstreeks te relateren is aan de dwarscontractie-coëfficiënt.

Het is mogelijk een eenvoudige buigproef uit te voeren, waarbij onderzocht kan worden wat het effect is van een zijdelingse drukspanning op de dwarscontractie-coëfficiënt van beton dat onderworpen is aan een gelijkmatig verdeelde éénassige trekspanning.

In een ruitvormige plaat die in twee tegenovergestelde hoeken ondersteund en in de vrije hoeken belast wordt zal een anticlastische homogene buigspanningstoestand ontstaan.

Door het variëren van de verhouding van de diagonaallengten is het mogelijk vele spanningscombinaties te realiseren. Ook dan zou de dwarscontractie-coëfficiënt gebruikt kunnen worden bij het formuleren van een grenstoestand.

Door de toepassing van de Ligtenberg reflectiemoiré methode en een schaduwmoiré techniek op perspex zijn de mogelijkheden van deze moiré-technieken onderzocht.

Door de vervormingen tijdens een beproeving van beton te sturen kunnen grote waarden voor de rek bewerkstelligd worden, hetgeen resulteert in een dicht maar inhomogeen scheurpatroon. Daarom zijn moiré methoden die een integraal beeld van dit patroon kunnen geven zeer geschikt. Het vast te leggen verloop van de dwarscontractiecoëfficiënt kan gerelateerd worden aan het scheurvormingsproces. Met name de schaduwmoiré techniek biedt perspectieven bij gebruik van eenvoudige en goedkope apparatuur.

1. Introduction

Concrete is a composite and therefor inhomogeneous material which demonstrates only under relative small forces an elastic behaviour. As a result of the random composition of the components the random distribution of pores and micro cracks present in the unloaded condition, plain concrete demonstrates a quasi isotropic behaviour.

In case of a loading less than 20 - 30% of the prism strength, there is no markable effect on the structure of pores and micro cracks)[1,3,4,5,6,10,11]. Beyond this point this will extend gradually by the spreading of the individual cracks and the development of new ones. Registrating the deformations of the concrete prism under uniaxial compression forces over this first loading stage, one is primarily dealing with elastic (reversible) deformations. In fact the stiffness of the concrete prism will increase gradually because part of the pores and cracks will be closed under compressive forces, resulting in non linear elasticity.

Increasing the stress beyond this lower critical point will result in a relative increase in longitudinal and lateral deformations, which is caused mainly by nucleation of bond cracks between the coarse aggregate and the matrix)[3,5]. The increase in the orthogonal deformation components is almost proportional. Therefor Poissons' ratio will nearly maintain a constant value. A similar phenomenon can be observed in case of uniaxial tension testing.

If the stress is increased to a sufficient high level, called the initiation stress, a new crack mechanism will develop. Cracks running through the matrix and connecting bond cracks at the interface of the aggregate gradually will produce a continuous crack pattern)[3,4,5,8]. Because the risk of development of tensile stresses is largest perpendicular to the loading direction the spreading cracks will show a preference for this direction.

As a result beyond the initiation stress Poissons' ratio will increase in compression or decrease in tension when the stresses are raised)[4,7,12]. In literature this stage is also called the discontinuity point in the strain)[8,13,14]. Since continuous cracks are a necessary condition for rupture this discontinuity point constitutes a theoretical lower bound for the strength. This is the reason why the term lower critical stress is often used.

This lower limit of structural loosening can be localised at about 60 - 80% of the prism strength determined with a short time test)[1,4].

Poissons' ratio can be defined in the usual way as its secant's value ν_1 or its tangent value ν_2 (fig. 1). Here by ν_1 is related to the total deformations and ν_2 to the amount of increase in these deformations.

With increasing strain the volumetric strain and the secant's value of Poissons' ratio constitute affine curves)[4,7]. At first the total volume of the prism decreases proportional to the strain, but beyond the discontinuity point the increasing crack density will gradually constitute a compensation which will finally give rise to an increasing total volume. The stress associated with the minimum value of the total volume is called the critical stress. It follows from experimental investigations that the strength of plain concrete under permanent loading can be defined by this critical stress value. However it is possible to produce lower strength values for plain concrete subjected to dynamic loading.

Because in a prism a considerable amount of continuous cracks will develope, under an uniaxial critical stressfield, the literature indicates this point as the upper limit of structural loosening or the point of extensive internal cracking)[1]. It can be localised at about 70 - 90% of the prism strength determined with a short time test. The derivative of the volumetric strain with respect to the increasing

Fig. 1. Deformation parameters

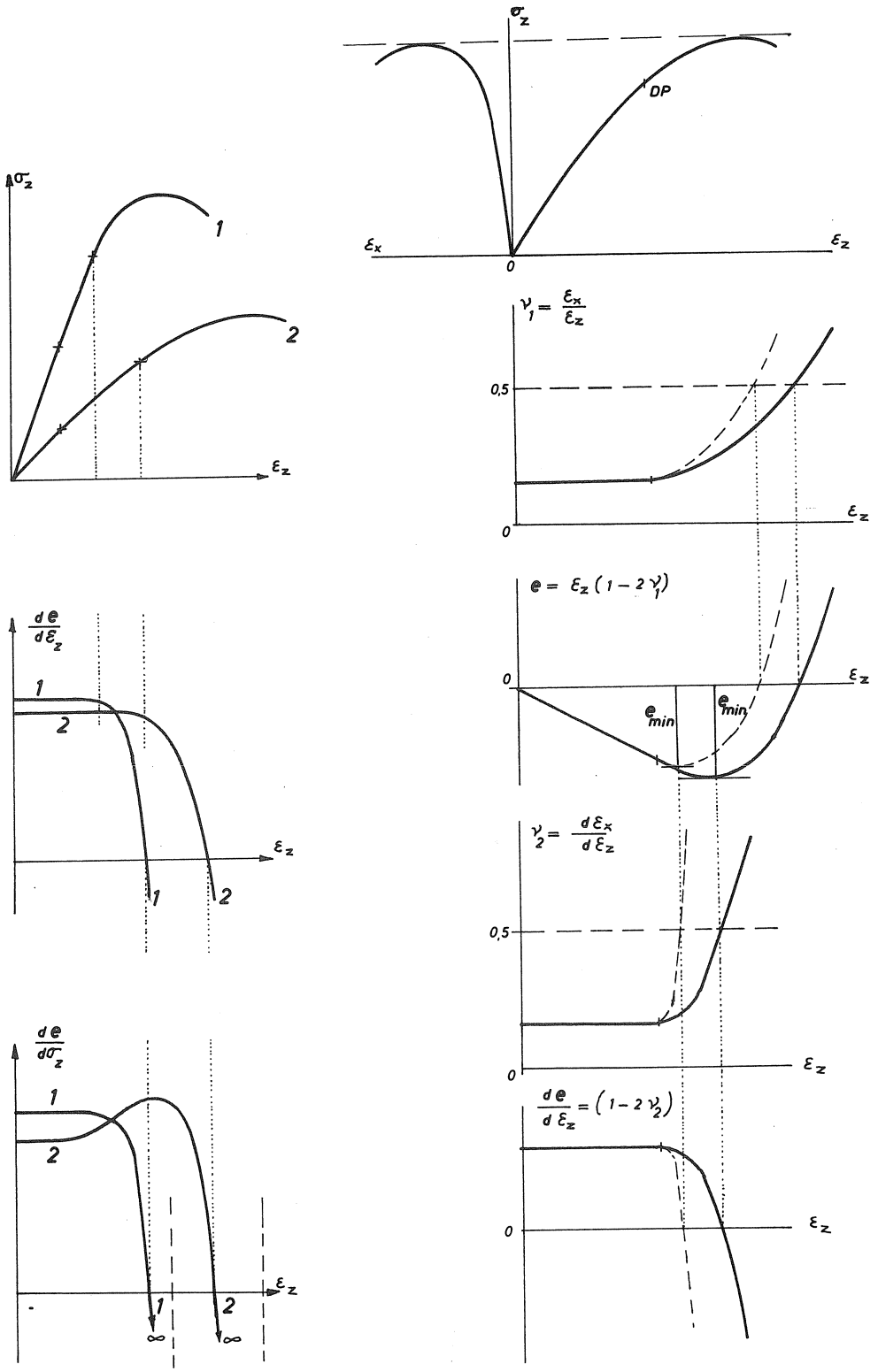

strain can be related directly to the tangent value of Poissons' ratio)[4,7,8]. Beyond the lower critical stress (discontinuity point) a considerable deflection can be observed in these curves)[11].

As it follows from the above Poissons' ratio can be an important parameter to define the strength of plain concrete. In the "elastic range" a physical meaning can be attributed to this and other related quantities. Beyond the lower critical stress this physical meaning becomes obscured, but it can be transformed into a new one characterising the crack system. In this way the before mentioned derivative of the volumetric strain can be associated with the crack density)[4,15,16]. In the uniaxial and biaxial state of stress the deformations are comparatively large, the explorations numerous. In the corresponding tensile state of stress the deformations are more than one order in magnitude smaller)[2,9,10]. Therefore, one must exact a high standard of reliability which includes a high sensitivity, but also a large measuring range.For high strains can be achieved by controlling the deformations during testing)[9, 10]. In addition, there is the difficulty of the discreteness of the crack development process, which will give preference to a full field measuring method.

The two measuring methods, which will be discussed here, are applied at the Stevin laboratory during an experimental program on folded plate constructions)[17].

Six reinforced folded plate constructions were tested during $2\frac{1}{2}$ years. After 10, 28 and 42 days prismatic disc shaped testspecimen were subjected to a variety of loading systems. The testspecimen were fabricated by use of the shotcrete technique like the shell itself.

Fig. 2. Uniaxial tension test specimen after rupture

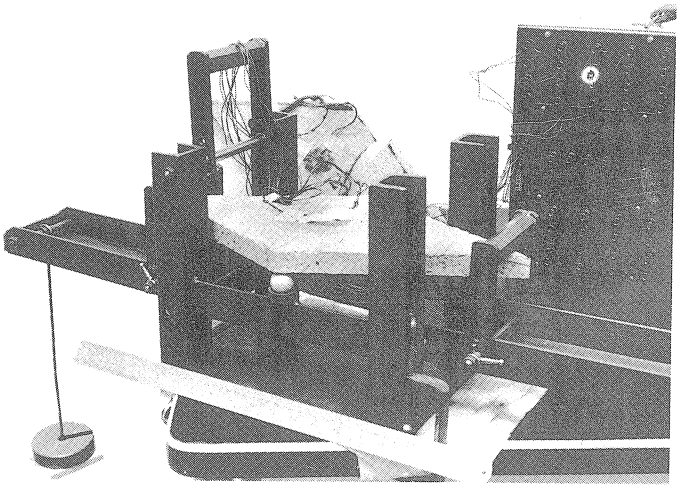

Fig. 3. Rhombic plate experiment Specimen of microconcrete

All the specimen were sawed from plates having the same thickness (1") as the model of the shell. The dimensions of the uniaxial tension specimen were 1" x 3" x 6". They were glued with epoxy to steel heads. The tensile load could be introduced by rods which were screwed in the heads (fig. 2). This arrangement is analogous to a method worked out by Kadleček and Špetla in response to an inquiry of RILEM)[18,19].

The rhombic plate dimensions are: thickness 1", diagonal length 9" and 18". The loading was applied by dead load in a simple bending apparatus (fig. 3).

Fig. 4.

Optical measuring device
l=leverarm
1.specimen
2.knife
3.correction screw

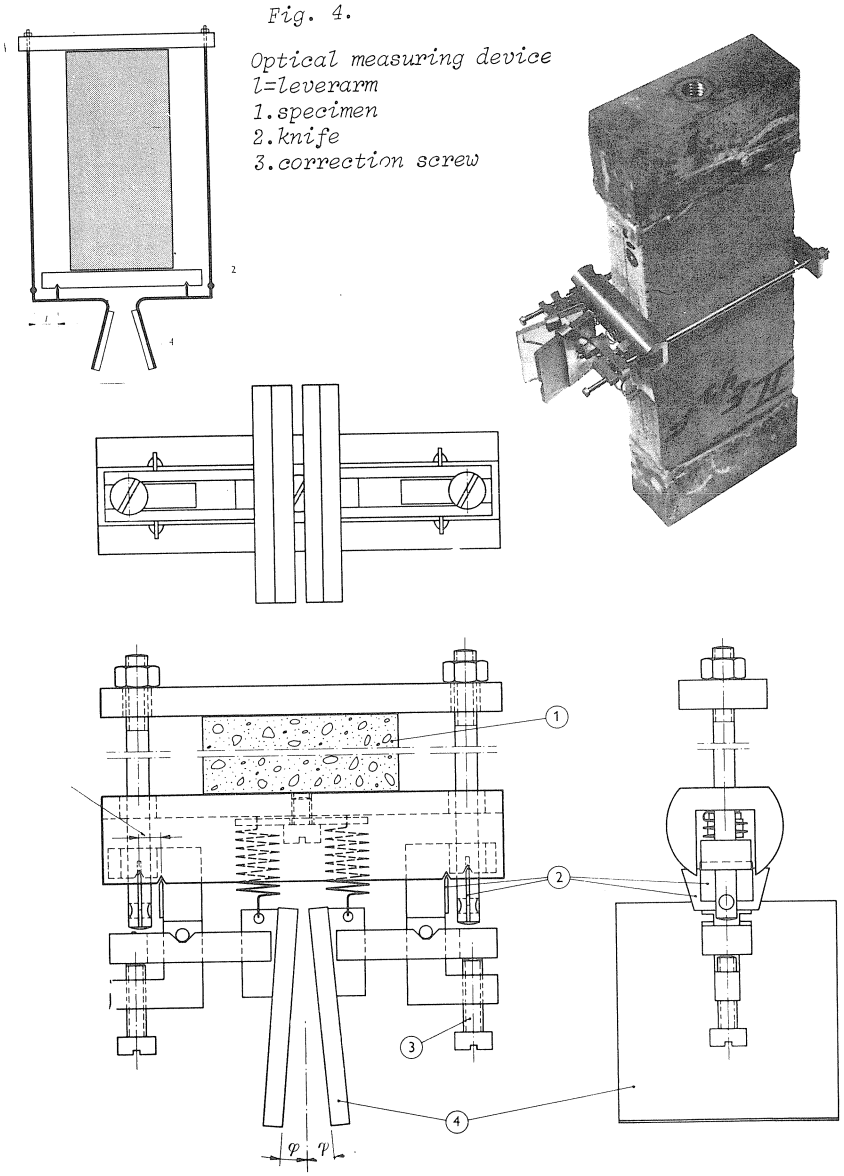

2. Uniaxial tension test - Optical measuring device)[20]

To allow for the tangential deformations to be registrated an optical measuring device has been conceived and constructed (fig. 4).
By mechanical means the dilatation in the middle section of the testspecimen is transformed into rotation of two mirrors with small angular spacing. The mirror system provides a large increase of this rotation by plural reflection of a lightbeam within this system.

On one side, this offers the possibility of detecting tenth of microstrains (i.e. 10^{-7}), on the other hand, a measuring range up to 500 μstr. is within reach. Like other, similar optical devices)[21,23] it comprises of two small mirrors, but the system is compact and the angular spacing (2ϕ) is small ($\sim 10^{o}$).

The apparatus is composed of the following parts:

a. two clamping plates and two rods, together forming the frame which embraces the testspecimen. The rods are fixed at one end of a leversystem. The leverarm (l) is small (3,2 mm).

b. two mirrors which are connected with the hinge of the leversystem.

The dilatation (Δb) of the testspecimen is transformed into a rotation ($\Delta\phi$) of both mirrors. In this way, a light beam entering the system undergoes a considerable change in direction (θ_n) after a number of reflections (n) (fig.5) The image, formed by the light beam on a screen a distance (L) behind this system, has changed its position (s) by a shift (Δs) perpendicular to the light beam.

The following simple relationship gives a full description of this transformation procedure:

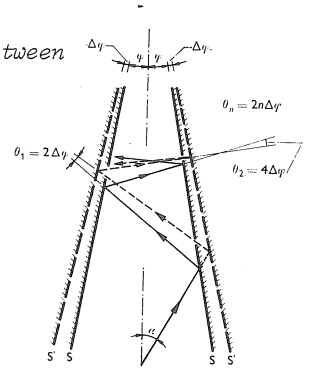

Fig. 5. Relation between θ_n and φ

$$\Delta s = \frac{2nL}{l}\,\Delta b = \frac{2nbL}{l}\,\varepsilon_t \qquad -1-$$

(t = tangential)

The original phenomenon (b) is multiplied by a factor V given by:

$$V = 2n\,\frac{L}{l} \qquad -2-$$

If L = 5000 mm and n = 16 a shift Δs can be observed, which surpasses Δb by a factor V = 50000

For a minimum shift of 0,1 mm and a width of the specimen of 7,5 cm (1) gives a measurable strain of 0,025 μstr. ($\frac{1}{4}.10^{-7}$), indicating the sensitivity of the method under these circumstances. The increase of the loading of the testspecimen, corresponding to this strain increment, is about 1 kg.

3. Testarrangement

The testarrangement can be realised in different ways:

1. by using a laser or conventional lightsource an image of wires is formed on a screen. In the latter case a system of lenses is necessary.
2. by using an illuminated ruler, which can be observed by a telescope standing in front of the mirror system. This method is employed in the Stevin laboratory (fig. 6).

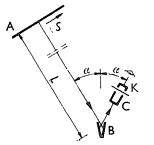

Fig. 6. Testarrangement
A lighted ruler
B optical measuring device
C telescope
K wires
L distance screen-optical system

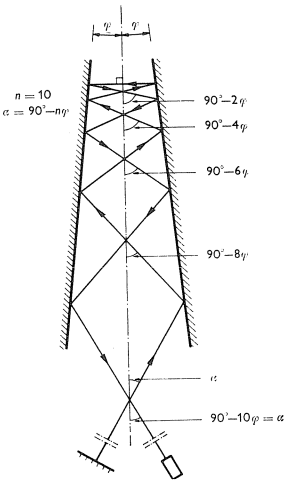

Fig. 7.
Multiple reflection of lightbeam within mirror system

The angle of adjustment of the telescope (α) together with the angular spacing of the mirror system (2ϕ) determines the maximum number of reflections which is obtainable under these circumstances. The quantities mentioned are related by (fig. 7):

$$\alpha = 90^{\circ} - n\phi$$

4. Experimental results

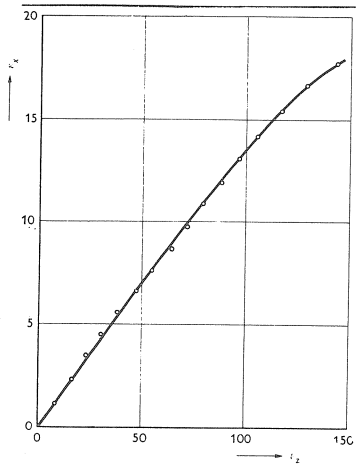

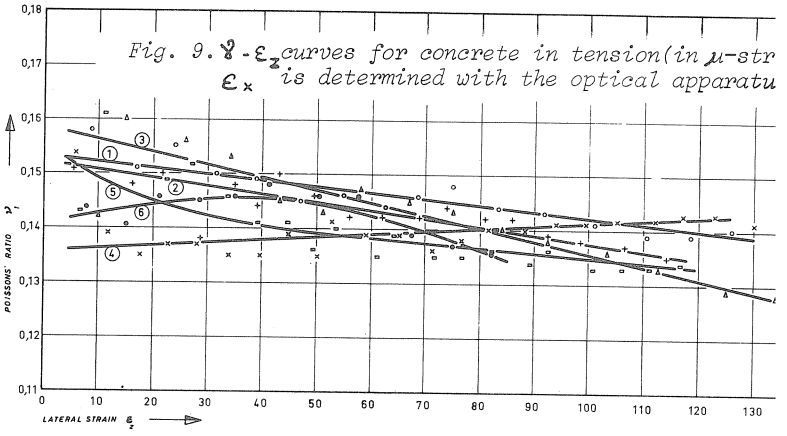

Fig. 9. ν-ε_z curves for concrete in tension (in μ-str ε_x is determined with the optical apparatu

Fig. 8. ε_x-ε_z curves for concrete in tension (in μ-str) ε_x is determined with the optical apparatus

Figures 8 and 9 give some experimental results extracted from the folded plate program mentioned earlier. It was impossible to perform the experiments in climatised surroundings. Yet reliable results are obtained. Because of the dead weight loading high strain could not be achieved.

5. Rhombic plate - basic formulae)[22]

According to the classic test of Nadai the determination of the flexural rigidity K is possible by anticlastic bending of a square plate.

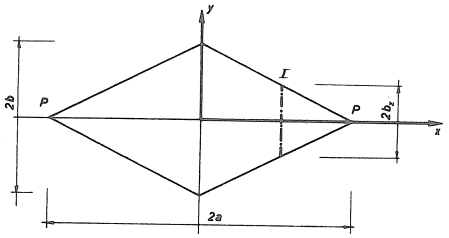

Fig. 10. Rhombic plate experiment

Performing an analogous test on a rhombic plate (or parallelogram) (fig. 10), not only the K-factor can be obtained but also Poissons' ratio. In the former case the diagonal length ratio ($\frac{b}{a}$) equals 1. In the other extreme, were $\frac{b}{a}$ tends to infinity, the rhombic plate degenerates to a long strip (or beam). Nevertheless determination of K and ν is possible but to introduce a homogeneous stress field is difficult.

In mathematical elasticity theory for thin plates with small deflections the curvature tensor components in the direction of the diagonals

of the rhombic plate are given by:

$$\chi_1 = \chi_{xx} = -P\left(\frac{a}{b} + \nu\frac{b}{a}\right)/2K(1-\nu^2) = -C\left(\frac{a}{b} + \nu\frac{b}{a}\right) \qquad -4a-$$

$$\chi_2 = \chi_{yy} = +P\left(\frac{b}{a} + \nu\frac{a}{b}\right)/2K(1-\nu^2) = +C\left(\frac{b}{a} + \nu\frac{a}{b}\right) \qquad -4b-$$

$$\chi_{xy} = \chi_{yx} = 0$$

Thus the (x,y) coordinate system is orientated in the direction of the axes of principal curvature. For an orthogonal coordinate system (u,v) with the u-axis parallel to one of the sides of the rhombic plate, the following relations are obtained:

$$\chi_{uu} = -P\left(\frac{a}{b} - \frac{b}{a}\right)/2K(1-\nu^2) = -C\left(\frac{a}{b} - \frac{b}{a}\right) \qquad -5a-$$

$$\chi_{vv} = +\nu P\left(\frac{a}{b} - \frac{b}{a}\right)2K(1-\nu^2) = +\nu C\left(\frac{a}{b} - \frac{b}{a}\right) \qquad -5b-$$

$$\chi_{uv} = \chi_{vu} = -P/2K(1-\nu) = -C(1+\nu) \qquad -5c-$$

The elastic plane is obtained after double integration of (4) or (5). In the (x,y) system:

$$w(x,y) = -\tfrac{1}{2}C\left[\left(\frac{a}{b} + \nu\frac{b}{a}\right)x^2 - \left(\frac{b}{a} + \nu\frac{a}{b}\right)\right]y^2 \qquad -6-$$

After substitution of:

$$tg^2\phi = \frac{\nu + tg^2\phi}{1 + \nu tg^2\phi} \qquad -7-$$

with:

$$tg\ \phi = \frac{b}{a},$$

the following simple relation results from (6):

$$w(x,y) = C_1\,(x^2 - tg^2\phi\ y^2), \qquad -8-$$

in which:

$$C_1 = -\tfrac{1}{2}C\,(1 + \nu tg^2\phi)\ \mathrm{cotg}\ \phi \qquad -9-$$

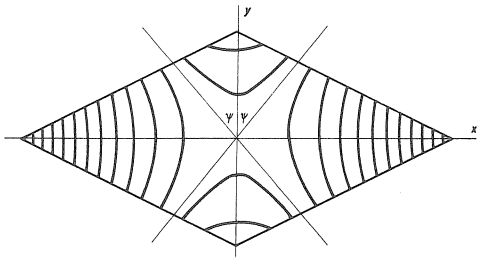

Fig. 11. Deflection contours

And analogous for the (u,v) system:

$$w(u,v) = C_2 \left[u^2 + (1 + \nu)\, tg^2\phi\, uv - \nu v^2 \right], \qquad -10-$$

with:

$$C_2 = - C \cot g\, 2\phi$$

For constant values of w (8) of (10) represents two systems of hyperbolic lines. The asymptotic lines enclose angles ψ with the y-axis (fig. 11). The edges of the rhombic plate are curved in the shape of hyperbolic lines (viz. (10) with $v = b \sin \phi$). Furthermore if (8) is transformed to a coordinate system (s,t) with axes oriented in the direction of the asymptotic lines, the elastic plane can be described by (fig. 12):

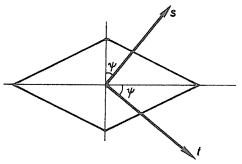

Fig. 12. (s,t)coordinate system

$$w(s,t) = 4\, C_1 \sin^2\psi\, s.t, \qquad -11-$$

which is the formula of an oblique hyperbolic paraboloid. The straight lines are ruled parallel to the s- and t-axes.

The elastic plane can be defined by an other system of lines, i.e. lines of constant rotation (grad. w). In a simple way, one can deduce)[22,23]:

$$(\text{grad. } w)^2 = 4C_1^2 \left(x^2 + tg^4\psi\, y^2\right),$$

or in its basic form:

$$x^2 \Big/ \left[\frac{\text{grad. } w}{2C_1}\right]^2 + y^2 \Big/ \left[\frac{\text{grad. } w}{2C_1\, tg^2\psi}\right]^2 = 1, \qquad -12-$$

which is a system of ellipses for constant values of grad. w. The diagonal length ratio $(\frac{b'}{a'})$ of the principal axes of an arbitrary ellipse, will yield:

$$\frac{b'}{a'} = tg^2\psi \qquad -13-$$

6. Application to a long strip (or beam) and square plate)[23,24,25]

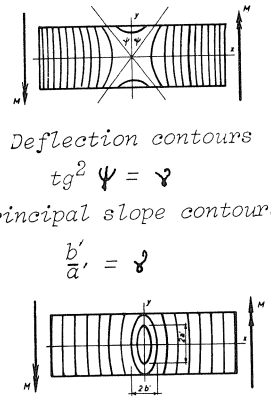

Deflection contours

$tg^2 \psi = \nu$

Principal slope contours

$\frac{b'}{a'} = \nu$

Fig. 13. Pure bending of strip

1. Strip or beam ($\phi \to 0$)

   ψ follows from (7):

   $tg^2\psi = \nu$

   Together with (8) and (13) a very simple way of determining ν is achieved (fig. 13).

2. Square plate (Nadai))[23,25] ($\phi = \pi/4$)

   ψ follows from (7):

   $tg^2\psi = 1$

   The hyperbolic lines constitute an orthogonal system and offer no information concerning ν . In this case (12) is reduced to a system of equidistant circles (fig. 14)

Deflection contours

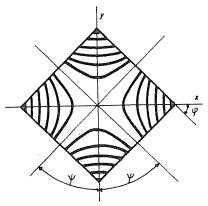

Fig. 14. Anticlastic bending of square plate

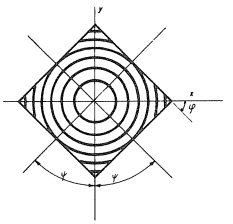

Principal slope contours

7. Application to the rhombic plate

In case a moiré picture of deflection contours is available Poissons' ratio can be deduced along different ways:

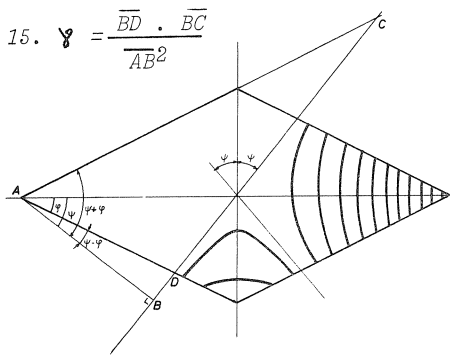

Fig. 15. $\nu = \frac{\overline{BD} \cdot \overline{BC}}{\overline{AB}^2}$

(a_1) by measuring the angle ψ formed by the asymptotic lines of the deflection contours and the y-axis (fig. 11)

(a_2) semigraphical. (7) can be written in the form:

$\nu = tg\,(\psi + \phi) \cdot tg\,(\psi - \phi)$, -14-

which leads to (fig. 15):

$$\nu = \frac{\overline{BD} \cdot \overline{BC}}{\overline{AB}^2}$$

(a_3) by deducing tg ψ from the coordinates of two or more points on the same deflection contour.

For two points S and T it follows from (8) that:

$$tg^2\,\psi = \frac{x^2_s - x^2_t}{y^2_s - y^2_t} \qquad -15-$$

(a_4) with an arbitrary number of points on any deflection contour the same procedure can be applied. Using three points P, Q and R it follows from (8) that:

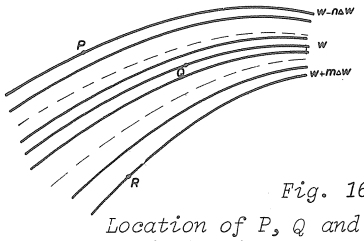

Fig. 16.
Location of P, Q and R on deflection contours.

$$tg^2\,\psi = \frac{(m+n)\,x^2_q - m\,x^2_p - n\,x^2_r}{(m+n)\,y^2_q - m\,y^2_p - n\,y^2_r}, \qquad -16-$$

in which P and R are situated on the n^{th} and m^{th} deflection contour respectively at different sides of the one passing through Q (fig. 16).

In case of a conveniently situated pattern of points a_3 and a_4 give an accurate mean of ν over the surface.

(a_5) by optical differentiation of the former moiré picture (Moislim process) a second order pattern of partial slope contours, comprising equidistant straight lines, will originate, offering an easy method to determine Poissons' ratio.

In case a moiré pattern of <u>rotation</u> (partial or principal) <u>contours</u> is available, Poissons' ratio can be deduced along different ways:

(b_1) the quotient of the principal curvature components leads to:

$$\frac{\chi_2}{\chi_1} = - tg^2\psi$$

χ_2 and χ_1 can be related in the generally known manner to certain intervals of the partial slope contours.

(b_2) in a similar way for the (u,v) coordinate system:

$$\frac{\chi_{vv}}{\chi_{uu}} = - \nu$$

A check on accuracy of the patterns is possible via $\chi_{uv} = \chi_{vu}$

(b_3) from (10) can be deduced that:

$$\frac{\partial}{\partial u} w(u,v) = 2C_2 (u + tg\ \gamma_1 v) \qquad -17a-$$

$$\frac{\partial}{\partial} w(u,v) = C_2 (1 + \nu)\ tg^2\ 2\ \emptyset\ (u + tg\ \gamma_2 v), \qquad -17b-$$

in which:

$$tg\ \gamma_1 = \tfrac{1}{2} (1 + \nu)\ tg\ 2\ \emptyset$$

$$tg\ \gamma_2 = -\ 2\nu\ /(1 + \nu)\ tg\ 2\ \emptyset \qquad -18b-$$

The product of (18a) and (18b) directly produces Poissons' ratio:

$$tg\ \gamma_1 .\ tg\ \gamma_2 = -\ \nu \qquad -19-$$

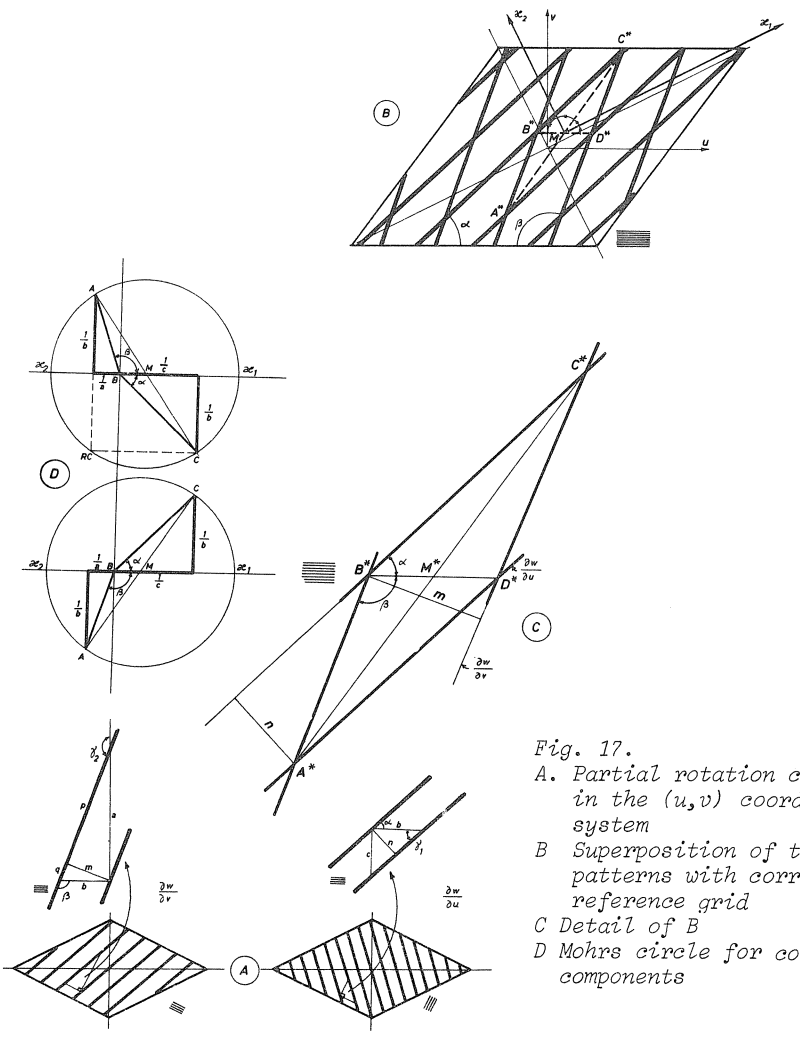

Fig. 17.
A. Partial rotation contours in the (u,v) coordinate system
B Superposition of these patterns with corresponding reference grid
C Detail of B
D Mohrs circle for corvature components

Determination of ν is possible by measuring γ_1 (via 18a), γ_2 (via 18b) or both (via 19) in separate patterns of the partial slope components (fig.17)

(b_4) a pattern of principal slope contours can be interpreted as indicated by (13))[27].

(b_5) a nice,elegant, yet simple method with a good check on accuracy is the next one:

Superpose the two partial slope contour patterns as described by (17a) and (17b) in such a way, that the reference grids will coincide. Because the original patterns consist of straight equidistant lines the resulting pattern presents a system of identical parallelograms Such a parallelogram $\overset{****}{ABCD}$ has outstanding features :

1. the diagonal $\overset{***}{AB}$ and the reference grid lines have corresponding directions.
2. the bisectrices of the angles between the two diagonals coincide in their direction with the angles of principal curvature.
3. the diagonal length ratio is related to Poissons' ratio)*:

$$m = \frac{\overline{DB}^{*}}{\overline{CA}^{*}} = \frac{\chi_1 + \chi_2}{\chi_1 - \chi_2} = \frac{1 - tg^2\psi}{1 + tg^2\psi} = \frac{1 - \nu}{1 + \nu} \cos 2\emptyset \qquad -20-$$

and in explicite form:

$$\nu = \frac{\cos 2\emptyset - m}{\cos 2\emptyset + m} \qquad -21-$$

8. Experimental techniques to determine Poissons' ratio

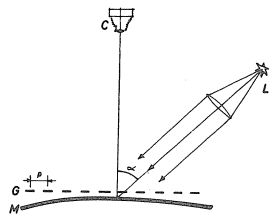

Fig. 18. Principle of shadow moire technique

a. via deflection contours

a_1: shadow moiré intensity interferometry)[28]

A plane reference grid placed in front of the model will project its shadow pattern on the diffuse surface of the model. A camera will registrate this shadow pattern and the reference grid (fig. 18). A moiré picture originates giving deflection contours described by:

$$w = (2n + 1)\, p \,/\, 2 \operatorname{tg} \alpha, (n = 0,1,2.....) \qquad -22-$$

)* viz appendix.

where:

p = pitch of reference grid

α = angle of inclination of the light beam with respect to the camera.

The same phenomenon arises by projecting via a diaprojector a grid on the surface. The deflection contours are described by:

$$w = (2n + 1)\ p\ /\ 2 \sin \alpha (n = 0,1,2.....) \qquad -23-$$

a_2: as far as a reflecting surface is concerned, a moiré picture can be obtained by photographing a reference grid in front of the surface in an oblique direction as well as the reflected image of it. The deflection contours are described by:

$$w = (2n + 1)\ p\ /\ 4 \operatorname{tg} \alpha, \qquad -24-$$

but the photograph shows a perspective error.

a_3: diffraction moiré)[29,30].

If a diffraction grid is placed in front of the reflective surface of a loaded model and if a coherent bundle of parallel light is used then the photographic plate shows an interference pattern which demonstrates a high degree of similarity with the moiré pattern of the preceeding methods, although the physical phenomena are different. The sensitivity of this method can be very high.

b. <u>via rotation contours</u>

b_1: Salet Ikeda technique)[23].

A reference grid is projected by means of a system of lenses on the reflective surface of the model. The reflected light rays have to pass a diaphragm before they reach the photographic plate. Partial and principal slope contours can be obtained.

b_2: Ligtenbergs' reflection moiré method)[31].

A camera observes through an opening in a line screen the image of this screen in the reflective surface of a model. Superposition of the photographs under unloaded and loaded condition produce moiré fringes with the same amount of information as b_1. The method however is less sensitive ($\sim$ 5x).

The rotation component θ will be described by:

$$\theta = (2n + 1)\ p\ /\ 4a, \qquad -25-$$

where a = distance screen-model.

9. Experimental results)[22]

In the Stevin laboratory the experiments on microconcrete were preceeded by some experiments on black perspex to evaluate the shadow moiré method in relation to the Ligtenberg reflection moiré method which is for perspex a very handy method . In this scope the interpretation of the Ligtenberg moiré pictures on (u,v) coordinates and superimposed as described under b_5 (§ 7) is illustrative (fig. 19, 20, 21).

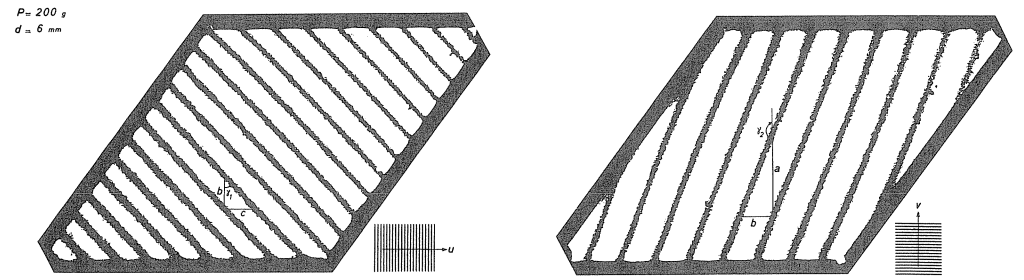

Fig. 19. Partial slope contours in (u,v) direction

Results from fig. 19: $\nu = -\frac{c}{a} \simeq 0{,}38$

$$\nu = -\operatorname{tg}\gamma_1 \operatorname{tg}\gamma_2 = \operatorname{tg} 43^\circ \operatorname{tg} 22^\circ 30' \simeq 0{,}39$$

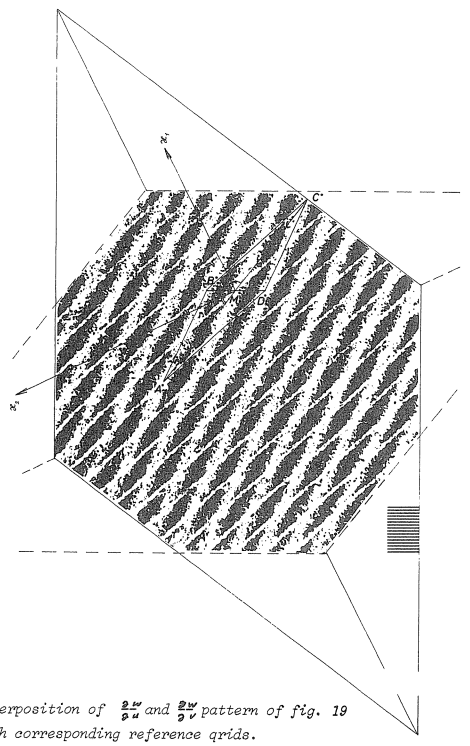

20. Superposition of $\frac{\partial w}{\partial u}$ and $\frac{\partial w}{\partial v}$ pattern of fig. 19 with corresponding reference grids.

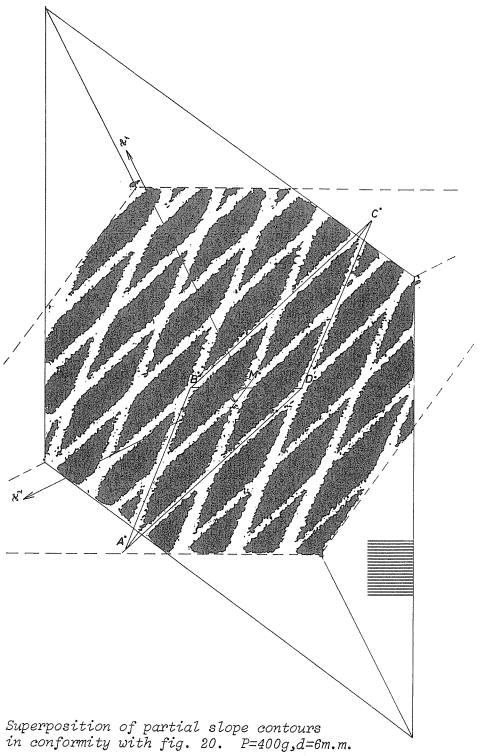

Fig. 21. Superposition of partial slope contours in conformity with fig. 20. P=400g,d=6m.m.

Results from fig. 20 : $m = 0{,}277$

$$\nu = \frac{0{,}6 - 0{,}277}{0{,}6 + 0{,}277} \simeq 0{,}37$$

fig. 21: $m = 0{,}265$

$$\nu = \frac{0{,}6 - 0{,}265}{0{,}6 + 0{,}265} \simeq 0{,}39$$

$$\nu = -\frac{c}{a} \simeq 0{,}38$$

$$\nu = + \operatorname{tg} 43^\circ \operatorname{tg} 22^\circ \simeq 0{,}38$$

According to the application on microconcrete the shadow moiré results are certainly as important as the former ones.

Fig. 22 and 23 give deflection contours for thin rhombic plates.

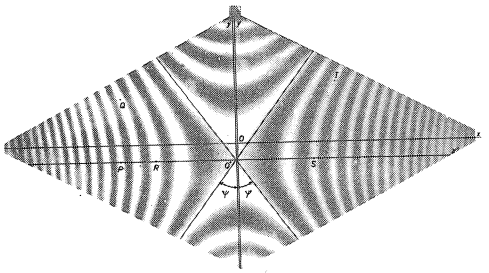

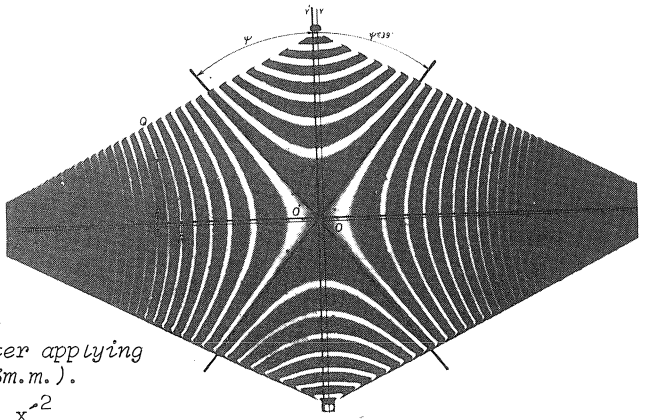

Fig. 22. Deflection contours P=500g, d=6m.m.

Fig. 23. Deflection contours after applying Schlieren process. (d=3m.m.).

Results from fig. 22: $\operatorname{tg}^2\psi = \dfrac{x'^2_s - x'^2_t}{y'^2_s - y'^2_t} = 0{,}564 \rightarrow \nu \simeq 0{,}38$

$\psi \simeq 37^\circ \rightarrow \nu \simeq 0{,}38$

Results from fig. 23: $\psi \simeq 39^\circ \rightarrow \nu \simeq 0{,}47$ (testarrangement incorrect)

via P, Q and R $\rightarrow \nu \simeq 0{,}47$

The photographs shown have been effected by very simple apparatus. A dia-projector served as light source. As a result of this the moiré picture will show some parallax moiré.

But using the method for microconcrete this phenomenon will not occur because of the very small deformations. Furthermore, the basic information needed was the change in Poissons' ratio and not its absolute value.

Introducing a small initial angle between model surface and grid, will result in a translation of the axes of symmetry of the deflection pattern. In this way an area with higher density in the moiré fringes can be recorded (fig. 24).

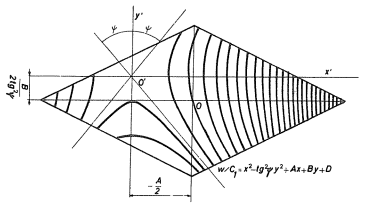

In this situation a transformation on new coordinate axes (x^1, y^1) which are situated symmetrically with respect to the moiré picture will produce an expression identical to (6), therefor misalignement will not influence the information.

Fig. 24. Deflection contours (with misalignement)

The moiré pictures can be interpreted in the sense as described in (a_1) to (a_5) (§.7). With respect to the methods (a_3), (a_4) and (a_5), it is necessary to make two comments.

Comment 1

By the transformation rule:

$$p = x^2 \qquad \text{-26a-}$$

$$q = y^2, \qquad \text{-26b-}$$

the hyperbolic lines in the deflection pattern will be transformed in a system of equidistant straight lines (fig. 25):

$$w = C_1 (p - tg^2 \psi . q) \qquad \text{-27-}$$

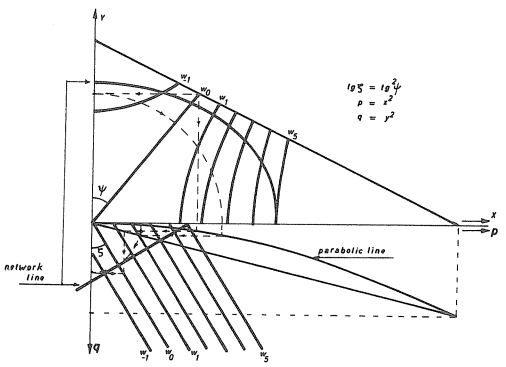

Fig. 25. Transformation op (pg) coordinate system

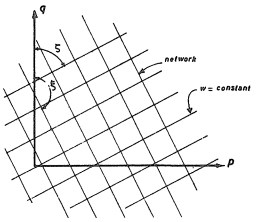

Fig. 26. Deflection contours and network pattern in the (pg) coordinate system.

A system of equidistant straight lines perpendicular to the lines given by (27) can be drawn in the (p,q) coordinate system (fig. 26). Transformed in the (x,y) system they constitute a system of ellipses (fig. 25).

The "conveniently situated points", as mentioned under a_4 can now be interpreted as the intersection of the hyperbolic lines and the ellipses. It is possible to construct this system of ellipses by accepting an arbitrary but expected value of Poissons' ratio.

A further possiblity is offered by the transformation of the w(x,y) pattern in the (p,q) coordinate system. The mean direction tangent (tg ζ) of the linepattern is directly related to ν.

$$\operatorname{tg}\zeta = \operatorname{tg}^2\psi = \frac{\nu + \operatorname{tg}^2\phi}{1 + \operatorname{tg}^2\phi}$$

Comment 2

It is possible to subject the deflection pattern to the moislim process)[26], producing partial rotation contours (fig. 27).

In addition to providing a check on accuracy, this method offers every possibility to evaluate Poissons' ratio as mentioned under b.

Results from fig. 27:

$\nu = 2\operatorname{tg}\gamma_1 \operatorname{cotg} 2\phi - 1 \simeq 0{,}48$

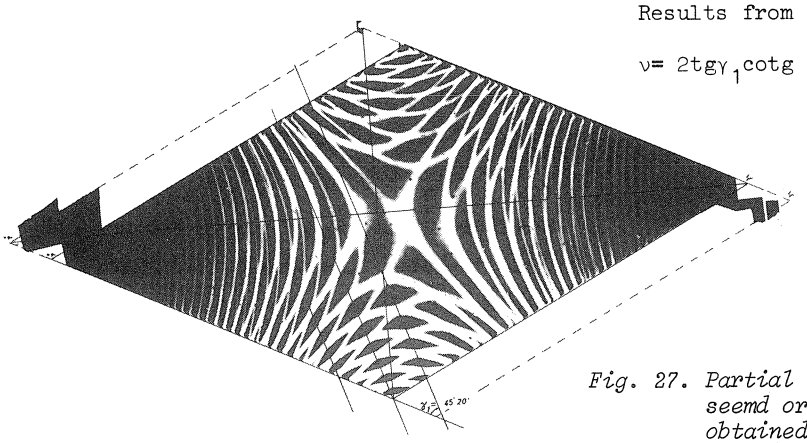

Fig. 27. Partial slope contours ($\frac{\partial w}{\partial x}$) seemd order moire picture obtained from fig. 23 after applying the moislim process

Literature

1. Desayi, L. Viswanatha, C.S. True ultimate strength of plain concrete. Rilem bull. nr. 36. sept. 1967.

2. Evans, R.H. Marathe, M.S. Microcracking and stress-strain curves for concrete in tension. Rilem bull. nr. 1, jan/febr. 1968.

3. Hsu, T.T.C. Slate, F.O. Sturman, G.M. Winter, G. Microcracking of plain concrete and the shape of the stress-strain curve. Journ. of the A.C.I., V.60 nr.2, febr. 1963.

4. Stroeven, P. The strength of concrete . Stev. rep. 5-68-7, june 1968 (in Dutch)

5. Jones, R. The development of microcracks in concrete. Rilem bull. nr. 9, dec. 1960.

6. Brace, W.F. Micromechanics in rock systems. Conf. on Struct. Solid mech. and Eng. design in Civ. Engs. mat., april 1969, Southampton.

7. Berés, L. Investigation on structural loosening of compressed concrete. Rilem bull. nr. 36, sept. 1967.

8. Stroeven, P. Report of Prague visit including lecture: The investigation of deformation parameters of concrete and the related measurement devices. Stev. rep. 5-68-10, july 1968.

9. Hughes, B.P. Chapman, G.P. The complete stress-strain curve for concrete in direct tension. Rilem bull. nr. 30, march 1966, and Mag. of concr. res., V. 18, nr. 54, march 1966.

10. Hughes, B.P., Chapman, G.P. The deformation of concrete and microconcrete in compression and tension with particular reference to aggregate size. Mag. of concr. V. 18, nr. 54, march 1966.

11. L'Hermite, R. What do we know about the plastic deformation and creep of concrete. Rilem bull. nr. 1, march 1959.

12. Weigler, H. Becker, G — Untersuchungen über das Bruch- und Verformungsverhalten von Beton bei zweiachsiger Beanspruchung Deuts. Auss. für Stahlbet. nr. 157.

13. Plowman, J.M. — Youngs' modulus and Poissons' ratio of concrete cured at various humidities. Mag. of concr. res. V. 15, nr. 14, july 1963.

14. Newman, K. — The structure and engineering properties of concrete. Proc. Int. Symp. on Arch dams, april 1964, Pergamon Press. 1965.

15. Jenkins, G.M. — The influence of fine micro fissures on mechanical properties. Conf. on Struct. Solid. Mech. and Eng. design in Civ. eng. mat., april 1969, Southampton.

16. Murzewski, J. — Random structure of a quasi-homogeneous material. Conf. on Struct. Solid. mech. and Eng. design in Civ. eng. mat., april 1969, Southampton.

17. Stroeven, P. — Six folded plate constructions test loaded to failure, I.A.S.S. Symp. on fold. pl. constr., sept. 1970, Vienna.

18. Kadleček, V. Špetla, Z. — Neue Prüfvorrichtung zur Ermittlung des Zugfestigkeit des Betons. Baustoffenindustrie V 9, nr. 3 1966.
and: Stavebnícky Časopsis. S.A.V. XV, nr. 45 1967.
Rilem bull. nr. 33, dec. 1966.
Acta Polytechnica I, 2, 1966.
S.N.T.L. Techn. digest Prague vol. VII nr.9, sept. 1965.
Betonsteinzeitung, H 4, 1967.
Beton, V 15, nr. 11, 1965.
Journ. of Mat. V 2, nr 4, A.S.T.M. 1967.

19. Inquiry results — Direct tensile test of concrete. Rilem bull. sept. 1963.

20. Stroeven, P. Voorsluis, H. — Optical method for measuring very small deformations. Heron 16, nr. 2, 1968 (in Dutch).

21. Antson , M. Newman, K. The effect of mix proportion and the method of testing on Poissons' ratio for mortars and concretes. Mag. of concr. res. V. 18, nr 56, sept. 1966.

22. Stroeven, P. Determination of Poissons' ratio by anticlastic bending of a rhombic plate. Stev. rep. 5-68-6, Aug. 1968 (in Dutch).

23. Duncan, J.P. Brown, C.J.E. Slope contours in flexed elastic plates by Salet-Ikeda technique. Exp. Mech. 1963.

24. Horrocks, D. Johnson, W. On anticlastic curvature with special reference to plastic bending. A literature survey and some experimental investigations. Int. journ. Mech. Sci. V 9, 1967.

25. Witteveen, J. The behaviour of plates under concentrated loads in their corner points. Heron 15, nr. 1, 1967 (in Dutch).

26. de Haas, H.M. Loof, H.W. An optical method to facilitate the interpretation of moiré pictures V.D.I. Ber. nr. 102, 1966.

27. Duncan, J.P. Sabin, P.G. Determination of curvatures in flexed elastic plates by the Martinelli Ronchi technique. Exp. Mech. dec. 1963.

28. Duncan, J.P. The optical survey of curved surfaces by intensity interferometry and related methods. Seminar Sheffield, 1966.

29. Middleton, E. A reflection technique for the survey of the deflection of flat plates. Exp. Mech. febr. 1968.

30. Ebbeni, J. Etude du phenomène du moirure par réflection d'un réseau plan sur une surface gauchie et de son application en analyse des contraintes et des déformations. V.D.I. Ber. nr. 102, 1966.

31. Ligtenberg, F.K. The moiré method. A new experimental method for the determination of moments in small slab models. Proc. S.E.S.A. vol. 12. nr. 2, 1955.

APPENDIX (viz. fig. 17)

$$\overline{AB}^2 = \frac{1}{a^2} + \frac{1}{b^2} = \left[\frac{\delta^2 w}{\delta v^2}\right]^2 + \left[\frac{\delta^2 w}{\delta u \delta v}\right]^2$$

$$= \left[\tfrac{1}{2}(k_{11} + k_{22}) - \tfrac{1}{2}(k_{11} - k_{22}) \cos 2\phi\right]^2 + \left[\tfrac{1}{2}(k_{11} - k_{22}) \sin 2\phi\right]^2$$

$$= \tfrac{1}{2}\left[(k_{11}^2 + k_{22}^2) - (k_{11}^2 - k_{22}^2)\cos 2\phi\right]$$

$$\overline{BC}^2 = \frac{1}{b^2} + \frac{1}{c^2}$$

$$= \tfrac{1}{2}\left[(k_{11}^2 + k_{22}^2) + (k_{11}^2 - k_{22}^2)\cos 2\phi\right]$$

+

$$\overline{AB}^2 + \overline{BC}^2 = k_{11}^2 + k_{22}^2 \qquad \text{(I)}$$

$$\overline{BM}^2 = \tfrac{1}{2}(\overline{AB}^2 + \overline{BC}^2) - \tfrac{1}{4}\overline{AC}^2 \qquad \text{(II)}$$

(I) and (II):

$$\overline{BM}^2 = \tfrac{1}{2}(k_{11}^2 + k_{22}^2) - \tfrac{1}{4}(k_{11} - k_{22})^2 = \tfrac{1}{4}(k_{11} + k_{22})^2$$

(form. 20):

$$\frac{\overline{DB}^*}{\overline{CA}^*} = \frac{\overline{DB}}{\overline{CA}} = \frac{k_{11} + k_{22}}{k_{11} - k_{22}} = \frac{\chi_1 + \chi_2}{\chi_1 - \chi_2}$$